THE JOURNAL OF BIOLOGICAL CHEMISTRY VOL. 282, NO. 11, pp. 7912–7920, March 16, 2007

In Vitro Analysis of *Sp*Ure2p, a Prion-related Protein, Exemplifies the Relationship between Amyloid and Prion*[S]

Received for publication, September 7, 2006, and in revised form, December 22, 2006 Published, JBC Papers in Press, January 17, 2007, DOI 10.1074/jbc.M608652200

Francoise Immel[‡1], Yi Jiang[§1], Yi-Qian Wang[§¶], Christelle Marchal[‡], Laurent Maillet[‡], Sarah Perrett[§2], and Christophe Cullin[‡3]

From the [‡]IBGC, UMR5095 CNRS-Université Bordeaux2, 1, rue Camille Saint Saens, 33077 Bordeaux cedex, France, the [§]National Laboratory of Biomacromolecules, Institute of Biophysics, Chinese Academy of Sciences, 15 Datun Road, Chaoyang District, Beijing 100101, China, and the [¶]Graduate School of the Chinese Academy of Sciences, Beijing 100039, China

The yeast *Saccharomyces cerevisiae* contains in its proteome at least three prion proteins. These proteins (Ure2p, Sup35p, and Rnq1p) share a set of remarkable properties. *In vivo*, they form aggregates that self-perpetuate their aggregation. This aggregation is controlled by Hsp104, which plays a major role in the growth and severing of these prions. *In vitro*, these prion proteins form amyloid fibrils spontaneously. The introduction of such fibrils made from Ure2p or Sup35p into yeast cells leads to the prion phenotypes [URE3] and [PSI], respectively. Previous studies on evolutionary biology of yeast prions have clearly established that [URE3] is not well conserved in the hemiascomycetous yeasts and particularly in *S. paradoxus*. Here we demonstrated that the *S. paradoxus* Ure2p is able to form infectious amyloid. These fibrils are more resistant than *S. cerevisiae* Ure2p fibrils to shear force. The observation, *in vivo*, of a distinct aggregation pattern for GFP fusions confirms the higher propensity of *Sp*Ure2p to form fibrillar structures. Our *in vitro* and *in vivo* analysis of aggregation propensity of the *S. paradoxus* Ure2p provides an explanation for its loss of infective properties and suggests that this protein belongs to the non-prion amyloid world.

The yeast prions represent an attractive and valuable model for understanding complex aspects of mammalian prion biology. The yeast system has provided the first experimental demonstration (1) of the "protein-only" concept proposed by J. Griffith (2) and developed by S. Prusiner (3) to explain the disconcerting biological properties of the infectious agent responsible for the transmissible spongiform encephalopathies. More recently, prions of *Saccharomyces cerevisiae* have offered a molecular explanation for the puzzling prion strain properties (4, 5). Apart from the power of budding yeast as a model for complex events involved in prion disease, the presence and the physiological role of these prions in yeast cells is itself a matter of interest and debate.

Yeast prions are not harmful to cells, and their presence does not lead to cellular death but rather to a loss of functional phenotype. The paradigm nevertheless remains the same: the protein undergoes a modification which leads to a change or a loss of function, and this modification occurs in an autocatalytic manner; the protein provoking its own conversion. In *S. cerevisiae*, the two best studied prions [URE3] and [PSI] correspond to the autocatalytic inactivation of Ure2p and Sup35p, respectively. Both proteins share a common organization with an N-terminal domain (termed the prion-forming domain or PFD[4] by R. Wickner (6)) only involved in the prion formation of the protein. The remaining part of the protein is able to complement the corresponding null mutant indicating that it represents the functional part of the protein.

Sup35p is a translation termination factor, and its partial inactivation causes the ribosomes to read through stop codons. Ure2p binds to the transcription factor Gln3p, preventing its migration to the nucleus (7). The interaction between Ure2p and Gln3p is a fundamental event in nitrogen catabolic repression (NCR). NCR is the physiological process by which selective use of available nitrogen sources is achieved. In the presence of excess nitrogen (a good nitrogen source in adequate supply) transcription of genes encoding the proteins needed to transport and degrade poor nitrogen sources does not occur. Conversely, when the amount of a good nitrogen source becomes limiting, or only poor nitrogen sources are available, the genes needed for their transport and catabolism are transcribed with the help of Gln3p.

The presence of [PSI] is usually assessed by the suppression a premature stop codon located in the *ADE1* gene. However, the presence of this prion has a broad effect and may affect positively or negatively the growth of the yeast cells, depending on the conditions used (8). This phenotypic plasticity led S. Lindquist to propose a role for [PSI] in the acquisition of new traits during evolution. As [PSI] is remarkably conserved in the

* This work was supported by grants from GIS "Infections à Prions" (to C. C.) and by the Natural Science Foundation of China (30470363, 30670428, 30620130109), the Chinese Ministry of Science and Technology (2006CB500703, 2006CB910903), the Chinese Academy of Sciences Knowledge Innovation Project (KSCX2-SW214-3), and by core funding from the Institute of Biophysics (to S. P.). The costs of publication of this article were defrayed in part by the payment of page charges. This article must therefore be hereby marked "*advertisement*" in accordance with 18 U.S.C. Section 1734 solely to indicate this fact.

[S] The on-line version of this article (available at http://www.jbc.org) contains supplemental Figs. S1–S5 and Table S1.

[1] Both authors contributed equally.

[2] To whom correspondence may be addressed. Tel.: 86-10-6485-6727; Fax: 86-10-6487-2026; E-mail: sarah.perrett@iname.com.

[3] To whom correspondence may be addressed. Tel.: 33-556-999-017; Fax: 33-556-999-01; E-mail: Christophe.Cullin@ibgc. u-bordeaux2.fr.

[4] The abbreviations used are: PFD, prion-forming domain; NCR, nitrogen catabolic repression; CHP, cumene hydroperoxide; CD, circular dichroism; GST, glutathione transferase; GPx, glutathione peroxidase; PK, proteinase K; *Sc*, *S. cerevisiae*; *Sp*, *S. paradoxus*; ThT, thioflavin T; GFP, green fluorescent protein.

hemiascomycetous phylum (9), this mechanism could be widely used by these unicellular organisms. In contrast, less is known about [URE3]. In previous work, we (10) and others (11) have isolated several orthologous *URE2* genes from different hemiascomycetous yeasts. We have then determined the capacities of these genes to complement the *URE2* function for NCR. We have also tested in *S. cerevisiae* the capacities of these different *URE2* genes to beget a prion phenotype. Interestingly, we found that this prion formation capacity was not maintained for the *S. paradoxus URE2* gene (*SpURE2*). *S. paradoxus* is an hemiascomycete yeast very closely related to *S. cerevisiae*. The two functional domains are identical, whereas the two PFDs exhibit only a few differences (supplemental Fig. S1). Interestingly, it was found that the *Sp*PFD has the capacity to induce the appearance of [URE3] (generated by *ScURE2*). This protein represents a paradox because it indicates that *Sp*Ure2p contains a PFD that is functional *in trans*, but not *in cis* (10). The inability of *Sp*Ure2p to switch into the inactivate prion isoform might be because of the lack of specific factors required for the prion formation mechanism in *S. paradoxus*. To gain insight into the conservation of this mechanism, we then engineered *S. paradoxus* by developing the genetic tools useful for the analysis of [URE3] (12). This work clearly demonstrated that only the primary sequence of *Sp*Ure2p contributes to the lack of prion properties.

Here, we characterize *Sp*Ure2p *in vitro*. We found that native and soluble Ure2p from *S. paradoxus* and *S. cerevisiae* have the same biochemical behavior. In both proteins, the PFD promotes efficient amyloidogenesis. The higher propensity of *Sp*Ure2p to form amyloid fibrils under more stringent conditions is the sole difference found. This characteristic reflects a less efficient fragmentation rate for *Sp*Ure2p that explains the incapacity for this protein to sustain [URE3]. To further test this hypothesis *in vivo*, we used GFP-tagged proteins to observe aggregates in [URE3] cells, and found clear differences in morphology, consistent with greater resistence to fragmentation of *Sp*Ure2p. Finally, we demonstrate that *Sp*Ure2p fibrils produced *in vitro* are infectious, confirming that the failure of *Sp*Ure2p to act as a prion stems from its inability to propagate transmissible prions *in vivo*, rather than a fundamental difference in amyloid structure.

EXPERIMENTAL PROCEDURES

Materials—GSH, β-NADPH, CHP, and glutathione reductase were from Sigma.

Construction of Ure2p Expression—The *URE2* open reading frame was PCR-amplified from pUHE-URE2 and cloned into pET3a resulting in pET3a-URE2. The 6× His tag was PCR-amplified and inserted at the 3′-end of *URE2* resulting in pET3a-URE2-His_6 (13). The full-length Ure2p *Sp* expression vector (pET-URE2 (*Sp*)-His_6) was obtained by amplifying by PCR a pUHE-URE2 (*Sp*) construct that encodes for Ure2p (*Sp*), using the following primers: 5′-CGGCATATGATGAATAACAACGGCAACC-3′ and 5′ -CCGCTCGAGTCATTCACCACGCAATGCC-3′. The amplified fragment was digested with NdeI and ligated into pET-URE2 (*Sc*)-His_6 digested using NdeI and NcoI.

The pYe2T-*sc*URE2GFP plasmid was originally described by Ripaud *et al.* (32). The pYe2T-*sp*URE2GFP was derived from the plasmids pYe2T-*sc*URE2GFP and pYe2T-*sp*URE2 originally described by Baudin-Baillieu *et al.* (10): a fragment coding the PFD domain of *sp*Ure2p was amplified by PCR using oligonucleotides (5′-TACATTAGGTCCTTTGTAGC-3′), binding the GAL10 promoter, and (5′-TGTTGTTCCAGCTGAGTATGC-3′), which introduces a Bsu36I restriction site a the 3′-end of the fragment. The PCR fragment was inserted into pYe2T-*sc*URE2GFP, between BamHI and Bsu36I sites, in place of the coding sequence of the *sp*Ure2p PFD domain.

Microscopy Techniques—AB34 cells (*MAT alpha, trp1-1, ade2-1, leu2-3, 112, his3-11, 15, ura2::HIS3* [URE3]) were transformed with pYe2T-*sc*URE2GFP or pYe2T-*sp*URE2GFP plasmids. Cells were grown overnight on YNB medium (0.67%) supplemented with raffinose (2%), appropriate amino acids, and USA (15 mg/liter). 2% galactose was then added to induce the Ure2pGFP expression. Aliquoted cells were pelleted at different times after galactose addition; and resuspended in DABCO solution (218 nM diazabicyclo 2-2-2 octane (Sigma), 25% (v/v) phosphate-buffered saline buffer, 75% (v/v) glycerol). Cells were observed and photographed with a DMRB microscope (Leïca, Germany) with a PL APO 63 objective).

Ure2p Expression, Purification, and Fibril Formation—Recombinant full-length Ure2p(*Sc*)-His_6 and Ure2p(*Sp*)-His_6 were overexpressed as soluble proteins in *Escherichia coli* BL21 codon+ DE3 strain (Stratagene) in LB medium containing 50 μg/ml ampicillin, 30 μg/ml chloramphenicol. Cells were grown to 0.8–1.0 A_{600} nm, and expression was induced by addition of 50 μg/ml isopropyl β-D-thiogalactoside. Induction was then performed overnight at 18 °C until the A_{600} nm reached 3.0–4.0. Recombinant full-length Ure2p(*Sc*)-His_6 was purified as previously described (14) with a modified buffer (20 mM Tris-HCl, pH 8, 300 mM NaCl) for the sonication.

The sonication of cells expressing the recombinant Ure2p(*Sp*)-His_6 was achieved in 20 mM Tris-HCl, pH 8, 50 mM NaCl + protease inhibitor mixture (complete EDTA-free, Roche Applied Science). The insoluble material was removed by centrifugation for 15 min at 20,000 × *g*, and the lysate was incubated with Ni-NTA resin (Qiagen) for 1 h at 4 °C. The resin was then washed with 50 mM NaCl, 20 mM Tris-HCl, pH 8, 20 mM imidazole. Protein elution was carried out in the same buffer containing 250 mM imidazole. The fractions containing Ure2p (*Sp*) were pooled, the NaCl concentration adjusted to 1 M, and applied to a HiTrap Phenyl HP (Amersham Biosciences) equilibrated in buffer A (20 mM Tris-HCl, pH 8, 1 M NaCl). The column was washed with equilibration buffer (buffer A) and developed with a first step of 35% buffer A, a second step of buffer B (20 mM Tris-HCl, pH 8), and finally a step of the buffer 20 mM Tris-HCl, pH 8, 10% glycerol.

Fractions emerging from the column in buffer B were pooled and concentrated with the help of a Centricon Plus-20 (Millipore). The typical yield was 30–40 mg of Ure2p(*Sc*)-His_6 and Ure2p(*Sp*)-His_6 per liter of culture. Alternatively, *Sc*Ure2p was produced with an N-terminal 6× His tag, using the vector mini-pRSETa, and purified under native conditions as described previously (15)The *Sp*Ure2p gene was also transferred from pET-URE2 (*Sp*)-His_6 to the mini-pRSETa vector to produce

*Sp*Ure2p with an N-terminal His tag. This was achieved using PCR using the following primers: 5′-ggccgcggatccatgaataacaacggtaaccaagtc-3′ (5′ primer containing BamH1 site) and 5′-ccgctcggggtaccttattcaccacgcaatgccttgat-3′ (3′ primer containing Kpn1 site). The amplified fragment was digested with BamH1 and Kpn1. The digestion product was then ligated into mini-pRSETa vector, digested with the same enzymes. The mini-pRSETa-URE2 (*Sp*) plasmid was transformed into *E. coli* C41 strain. The *Sp*Ure2p protein was then produced and purified as described above. The presence of N- or C-terminal His tags had no effect on the fibril formation behavior of either protein.

Size Exclusion Chromatography—The molecular size of the proteins was analyzed by chromatography on a FPLC Superose 12 column (Amersham Biosciences) equilibrated with 20 mM Tris-HCl, pH 8, 50 mM NaCl.

Filament Assembly—Fibrils were assembled for EM and PK analysis by incubating proteins (final concentration 75 μM) at 4 °C for 1–2 weeks without shaking in 20 mM Tris-HCl, pH 8, 300 mM NaCl for *Sc*Ure2p or 20 mM Tris-HCl, pH 8, 50 mM NaCl for *Sp*Ure2p. Filaments were purified by centrifugation (25,000 × *g*, 30 min) and washed at least two times with buffer before PK analysis.

Filaments were obtained in various buffers (20 mM Tris-HCl, pH 8, 50 mM NaCl, 50 mM Trehalose; 20 mM Tris-HCl pH 8, 50 mM NaCl, 100 mM NDSB-201; 20 mM Tris-HCl, pH 8, 50 mM NaCl, 1 mM glutathione; 20 mM Tris-HCl pH 8, 50 mM NaCl, 1 M TMAO; 20 mM Tris-HCl, pH 7, 50 mM NaCl.) The assembly of soluble full-length Ure2p was monitored by the measurement of sample turbidity expressed as optical density at 400 nm using a Cary 50 (Varian) spectrophotometer.

Electron Microscopy—Protein samples were loaded onto a copper grid coated with a Formvar film. To avoid rapid desiccation, sedimentation was allowed during a 10–30-min period in a moist Petri dish. Grids were then rinsed with 15–20 drops of freshly prepared 1% uranyl acetate in water (passed through a 0.22-μm filter, Millipore), dried with filter paper, and observed with a Phillips Tecnai 12 or Tecnai 20 electron microscope at 100 kV.

Limited Proteolysis—8 μl of a protein solution at 75 μM in 20 mM Tris-HCl, pH 8.0, 50 mM NaCl was mixed with 8 μl of appropriate dilutions of proteinase K (Promega), and incubated at 37 °C for 15 min. Digestion was stopped by the addition of electrophoresis sample buffer pH 6.8, containing 4% SDS, 2% mercaptoethanol (v/v), 12% glycerol (w/v), 0.01% Serva Blue G, and phenylmethylsulfonyl fluoride to a final concentration of 1 mM and immediately incubated at 100 °C for 5 min.

Digestion of amyloid fibrils was stopped by the addition of electrophoresis sample buffer, phenylmethylsulfonyl fluoride, and urea (to a final concentration of 8 M) and immediately incubated at 100 °C for 5 min.

Samples were analyzed by 15% SDS-PAGE. Gels were stained with Coomassie Blue or blotted to a nitrocellulose membrane (Optitran BA-S83, Schleicher & Schuell). Membranes were probed with specific affinity-purified polyclonal antibodies raised against full-length Ure2p.

Circular Dichroism Spectroscopy—The native conformation of soluble Ure2p(*Sc*)-His_6 and Ure2p(*Sp*)-His_6 was compared by circular dichroism spectroscopy. CD spectra were recorded in a 1-mm path quartz cell with a Jasco (Easton, MD) J-810 spectropolarimeter. All spectra were measured at 20 °C in 20 mM Tris-HCl, pH 8, 50 mM NaCl. Protein concentrations were 0.25 mg/ml, determined by absorption at 280 nm.

GdmCl Denaturation—1 μM protein was incubated overnight at 25 °C in 50 mM Tris-HCl, pH 8.4, 200 mM NaCl containing different concentrations of GdmCl before measuring the intrinsic fluorescence spectrum between 300 and 400 nm after excitation at 280 nm on a Shimadzu RF-5301PC spectrofluorimeter. The maximum change in fluorescence on denaturation was observed at 327 nm for both proteins. The plots were fitted to a three-state model as described (16).

ThT Assay—Fibril growth experiments and assay of ThT binding were performed essentially as described previously (16). 30 μM *S. paradoxus* and *S. cerevisiae* Ure2p were incubated in 50 mM Tris-HCl, pH 8.4, 200 mM NaCl at 10 °C on a MS2 Minishaker (IKA®) in a cold cabinet or at 37 °C in an Innova 4230-refrigerated incubator shaker (New Brunswick Scientific). (The stated pH of the buffer is correct at 25 °C.) A glass bead was added if the sample was shaken. Shaking speeds were as indicated in the figure legends.

Enzyme Assay and Steady-state Kinetic Analysis—The GPx activity of Ure2 was determined using GSH and CHP as substrates using a coupled spectrophotometric assay (17, 18). The assay was carried out at 25 °C in a 1-ml reaction volume containing 100 mM sodium phosphate buffer, pH 7.5, 0.15 mM β-NADPH and 0.24 units of glutathione reductase. Steady-state kinetic analysis was carried out. We measured k_{cat}, K_m, and V_{max} for *Sc* and *Sp*Ure2p to compare their activity. The k_{cat} value was measured using 1 mM GSH, and the Ure2 protein concentration was varied between 0.3 μM and 3.0 μM. The K_m and V_{max} values for 1 μM Ure2 were determined by varying the GSH concentration between 0.33 mM and 2.5 mM. The reaction mixture was preincubated at 25 °C for 4 min, after which the reaction was started by the addition of CHP to a final concentration of 1.2 mM. The progress of reactions was monitored continuously by following the decrease in NADPH absorbance at 340 nm on a Unico UV4802 spectrophotometer. Initial rates were determined from the linear slope of progress curves obtained with an extinction coefficient for NADPH of 6220 M^{-1} cm^{-1} after subtracting the non-enzymatic velocities caused by the auto-oxidation of GSH by the hydroperoxide determined from the corresponding blank. The data were fitted to the Michaelis-Menten equation. Single or global fitting was carried out using the regression wizard of SigmaPlot.

Assay of Ure2 GPx Activity during the Time Course of Amyloid-like Fibril Formation—The initial sample was centrifuged at 10,000 × *g* for 30 min at 4 °C to remove any preexisting aggregates, and 300 μl of the supernatant was transferred into each of a series of tubes, one for each time point. The reaction mixture contained 46 μM full-length *S. paradoxus* Ure2 in 50 mM Tris-HCl buffer, pH 8.4, containing 0.2 M NaCl. The samples were incubated in parallel at a constant temperature of 25 °C with shaking as described previously (16). Under these conditions, the increase in fluorescence caused by ThT binding correlates directly with the appearance of amyloid aggregates of Ure2. At each time point, one of the samples was placed on ice. Two 50-μl aliquots of the complete reaction mixture were

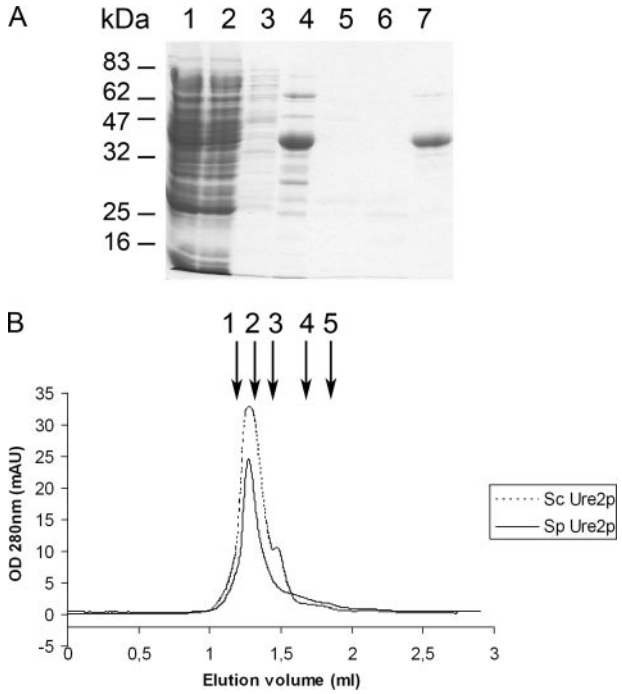

FIGURE 1. **Purification and characterization of recombinant *Sp*Ure2p.** *A*, expression and purification of Ure2p. Analysis on 12% SDS-PAGE at different steps of Ure2p purification. *Lane 1*, crude extract (soluble fraction). *Lane 2*, flow-through after binding on a Ni^{2+} column. *Lane 3*, wash. *Lane 4*, recombinant Ure2p emerging from the affinity chromatography column. *Lanes 5* and *6*, wash. *Lane 7*, recombinant Ure2p emerging from the hydrophobic chromatography column. *B*, size exclusion chromatography analysis of pure recombinant Ure2p. Elution profile of pure recombinant Ure2p from a Superose 12 column. *Arrowheads* show the location of molecular size markers: (*lane 1*, catalase, 232 kDa; *lane 2*, aldolase, 158 kDa; *lane 3*, bovine serum albumin, 67 kDa; *lane 4*, chymotrypsinogen, 25 kDa; *lane 5*, cytochrome *c*, 12.3 kDa).

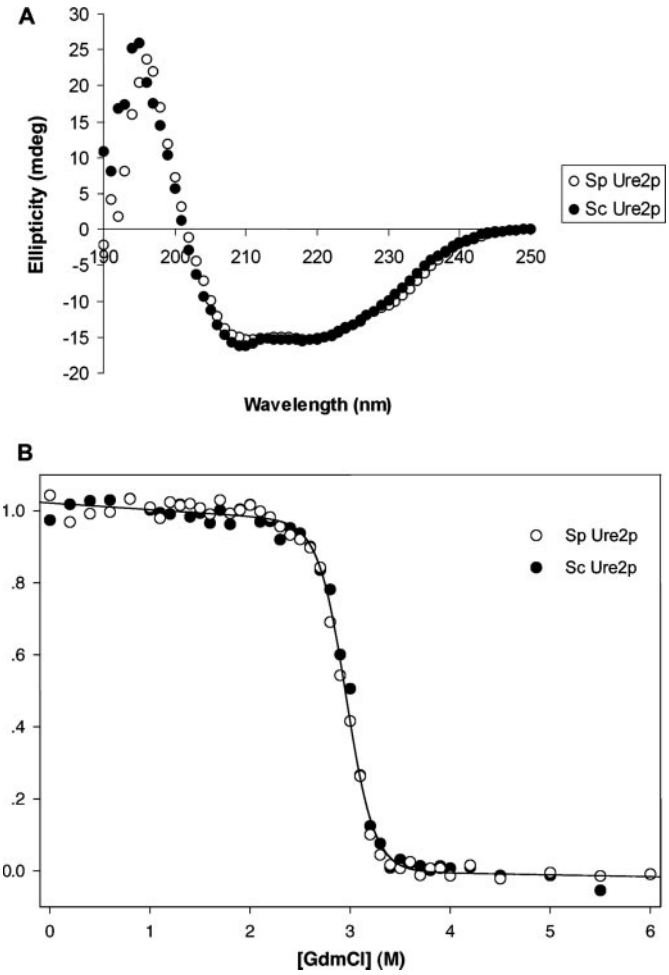

FIGURE 2. **Structure and stability of *Sp*Ure2p.** *A*, CD spectra of soluble *S. cerevisiae* and *S. paradoxus* Ure2p in 20 mM Tris-HCl buffer, pH 8, 50 mM NaCl. The protein concentrations were 0.25 mg/ml. *B*, GdmCl denaturation of *S. cerevisiae* and *S. paradoxus* Ure2p. Conditions were 1 μM protein concentration in 50 mM Tris-HCl, pH 8.4, 0.2 M NaCl containing different concentrations of GdmCl at 25 °C. Fitting of the data to a three-state model (16) gives the parameters shown in supplemental Table S2.

removed and assayed for GPx activity using 1 mM GSH and 1.2 mM CHP as substrates, as described above. A further 10-μl aliquot of the reaction mixture was removed to assay for ThT binding, as described previously (16). After centrifugation of the remaining 240 μl of sample, two 50-μl aliquot of the resulting supernatant were assayed for GPx activity. A further 10-μl aliquot of supernatant was used for protein concentration determination using the method of Bradford. The precipitate was resuspended in 240 μl of the same buffer, and then two 50-μl aliquots were assayed for GPx activity. Thus, the final protein concentration in the GPx assays was 2.3 μM for the total reaction mixture and a maximum of 2.3 μM in either the supernatant or the pellet fraction, depending on the relative distribution of protein between the fractions during the course of fibril formation. The values of GPx activity are mean values of two independent assays.

RESULTS

Purification of the Soluble Form of SpUre2p—After purification of the *Sp*Ure2 protein (see "Experimental Procedures"), a single species was observed that migrates with an apparent molecular mass of 42 kDa in SDS-PAGE (Fig. 1*A*). We next compared the behavior of recombinant *Sp* and *Sc*Ure2p by size exclusion chromatography (SEC). Both proteins eluted from the column in the same fraction indicating the same apparent molecular mass (Fig. 1*B*). This elution peak corresponds to a 160-kDa species, consistent with the previous results obtained with an untagged version of *Sc*Ure2p (14). This species has been shown to represent the dimeric form of the protein and was also observed for a His-tagged version of Ure2p (15). (The additional peak observed in the *Sc*Ure2p sample (Fig. 1*A*) corresponds to a contaminant polypeptide that is not systematically present in the *Sc*Ure2p-purified fraction and absent in the purest fraction of *Sp*Ure2p.) These data indicate that both *Sc* and *Sp*Ure2p assemble in the same way and show the same discrepancy between theoretical and experimental molecular mass by SEC.

Structure, Activity, and Stability of SpUre2p—Far-UV CD spectra (190–250 nm) of both proteins were then recorded (Fig. 2*A*). The two spectra clearly overlap, indicating a similar content of α-helix and the β-sheet in the two proteins. As the only differences between *Sc* and *Sp*Ure2p are found in the unstructured (1–94) part of protein, this means that there is no significant difference in the structure of the functional domains. The *Sc*Ure2p C-domain shows glutathione-dependent peroxidase activity, which is retained on formation of amyloid-like fibrils

TABLE 1

Apparent steady-state kinetic constants for *S. paradoxus* and *S. cerevisiae* Ure2p

The parameters were obtained by fitting the data shown in Fig. S2 to the Michaelis-Menten equation. CHP (1.2 mM) was used as the hydroperoxide substrate. Protein concentration was 1 μM.

	$K_{m(GSH)\ (app)}$	$V_{max(app)}$
	mM	s^{-1}
S. paradoxus Ure2[a]	2.4 ± 0.4	0.10 ± 0.02
S. cerevisiae Ure2[b]	2.4 ± 0.3	0.11 ± 0.01

[a] The errors shown are the S.E. of the fit.
[b] The values shown are the mean of three independent experiments, and the errors shown are the S.E.

(17). Here we compared the enzymatic activity of *Sc* and *Sp*Ure2p as a function of Ure2p concentration (supplemental Fig. S2), indicating that *Sp*Ure2p, like *Sc*Ure2p, shows Gpx activity and displays typical Michaelis-Menten kinetics (Fig. S3). The steady-state kinetic parameters obtained for the two proteins are the same within error (Figs. S1 and S2, and Table 1). These results indicate that both proteins are purified in a functional state and share the same enzymatic activity. We next examined the stability of these two proteins in the presence of the chaotropic agent guanidium hydrochloride (Fig. 2*B*). The equilibrium unfolding of Ure2p was recorded by following intrinsic fluorescence as a probe, under conditions where the stability of *Sc*Ure2p has already been studied in detail (15). *Sc* and *Sp*Ure2p showed identical equilibrium denaturation behavior (Fig. 2*B*) and fitting of the data to obtain thermodynamic parameters gave the same values within error (supplemental Table S1). These results suggest that the prion domains of *Sp* and *Sc*Ure2p contribute in the same way to the folding of the proteins.

*Aggregation Propensity of Sc and SpUre2p—Sc*Ure2p forms amyloid structures spontaneously that recapitulate all the properties considered typical of amyloids, namely: fibrillar morphology (19, 20), apple-green birefringence when stained with Congo Red (20), Thioflavin T binding (16, 21), proteinase K resistance of the fibril core (corresponding to the N-terminal domain (22)), and cross-beta structure of the fibril core (23). When incubated under standard conditions (20 mM Tris-HCl, pH 8, 50 mM NaCl, 20 °C without agitation), both proteins form macromolecular entities monitored by turbidity (Fig. 3). This technique is generally used to follow heat denaturation (24). Surprisingly, *Sp*Ure2p exhibits a higher propensity to aggregate than *Sc*Ure2p. These aggregates may stem either from ordered or disordered mechanisms. The use of electron microscopy definitively showed that the aggregates formed upon incubation correspond to fibrillar aggregates. As both proteins form such structures under standard conditions, we investigated different parameters that might affect specifically the fibrillation capability of one isoform. In the presence of trehalose (a

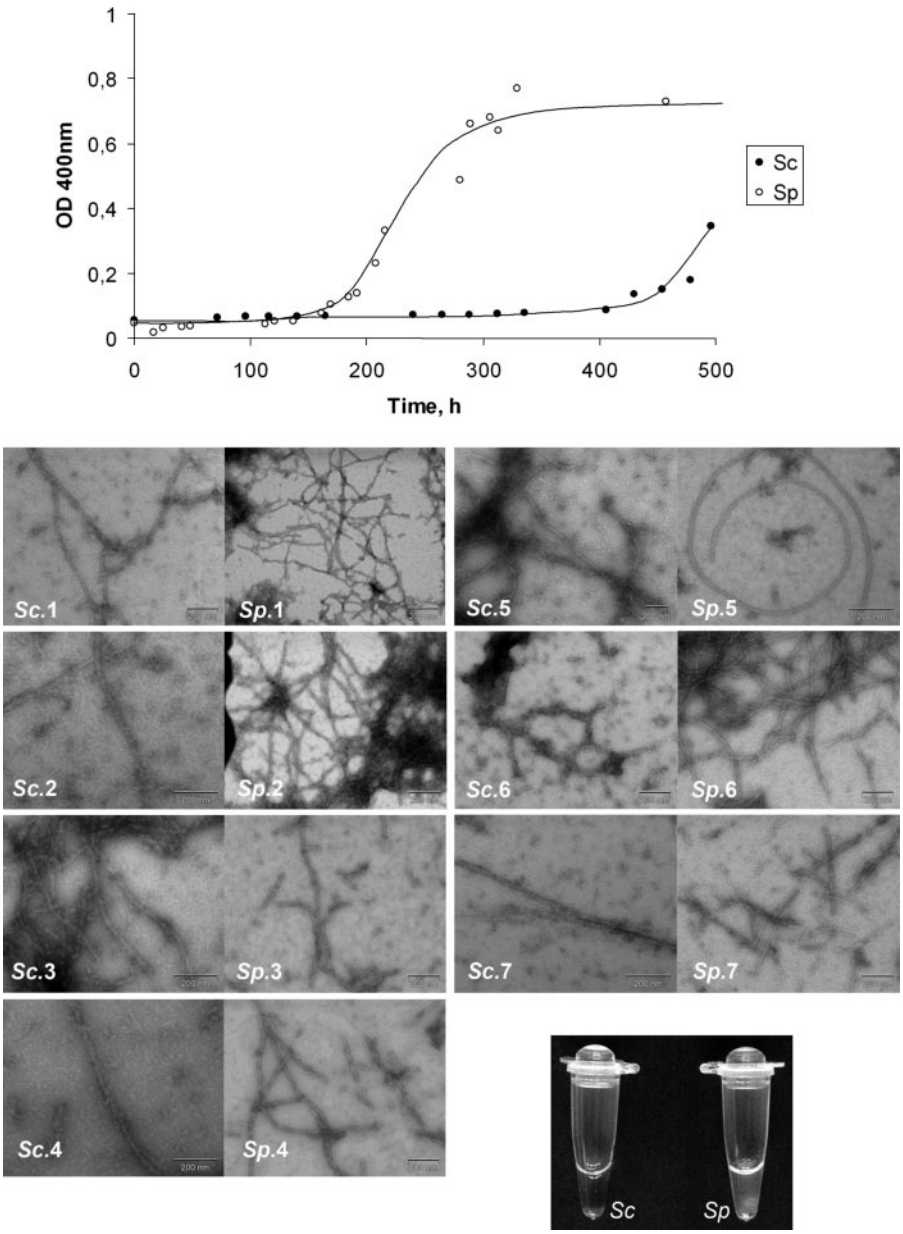

FIGURE 3. **Assembly of soluble full-length wild-type *Sp*Ure2p and *Sc*Ure2p in different buffers and identification of amyloid fibers.** Kinetics of protein assembly was monitored by turbidity measurement of the solution (expressed as optical density at 400 nm) at 20 °C in 20 mM Tris-HCl pH 8, 50 mM NaCl. The formation of amyloid fibrils from soluble *Sc* or *Sp*Ure2p in the following buffers was checked by negative staining electron microscopy. *Lane 1*, 20 mM Tris-HCl, pH 8, 50 mM NaCl. *Lane 2*, 20 mM Tris-HCl, pH 8, 50 mM NaCl, 50 mM Trehalose. *Lane 3,* 20 mM Tris-HCl, pH 8, 50 mM NaCl, 100 mM NDSB-201. *Lane 4*, 20 mM Tris-HCl, pH 7, 50 mM NaCl. *Lane 5*, 20 mM Tris-HCl, pH 8, 50 mM NaCl, 1 mM glutathione. *Lane 6*, 20 mM Tris-HCl, pH 8, 50 mM NaCl, 1 M TMAO. *Lane 7*, 20 mM Tris-HCl pH 8, 300 mM NaCl. *Bottom*, macroscopic observation of the final aggregates made with *Sp* or *Sc* Ure2p.

sugar that acts as a stabilizing agent (25)), non-detergent sulfobetaines NDSB-201 (a mild solubilization agent used for protein purification and renaturation (26)), the osmolyte trimethylamine N-oxide TMAO (a chemical chaperone that helps to maintain the structure of proteins (27)), glutathione (a tri-peptide substrate of Ure2p (17) that binds to the protein (28)) and at various values of pH and salt concentrations, *Sp*Ure2p still formed fibrillar structures in the same was as *Sc*Ure2p (Fig. 3). These structures appeared to be quite similar when observed on electron micrographs. However, the *Sp*Ure2p fibers were sometimes longer than *Sc*Ure2p fibers (see *Sp* + glutathione). Moreover *Sp*Ure2p typically formed cloudy aggregates, whereas this is less readily observed for *Sc*Ure2p (see Fig. 3).

Susceptibility to Proteolysis of Soluble and Fibrillar SpUre2p—*Sc*Ure2p filaments formed *in vitro* are clearly related to [URE3] because their introduction into yeast cells leads to the phenotypic switch characteristic of [URE3] (29). *Sp*Ure2p, although not competent to propagate this switch in yeast cells, is prone to form protein filaments that cannot be distinguished from *Sc*Ure2p infectious filaments by EM. We next examined in detail the main characteristics of these filaments. When *Sp*Ure2p filaments were subjected to proteinase K digestion used previously for digestion of *Sc*Ure2p filaments (13), they gave the same pattern on SDS gel with Coomassie Blue staining (Fig. 4*A*). We also compared this pattern to the profile obtained when soluble *Sp*Ure2p is used as the protease substrate under the same conditions. Interestingly, the profile obtained (Fig. 4*B*) is roughly the same and is consistent with the profile previously obtained when *Sc*Ure2p was subjected to limited proteolysis under identical conditions to those used here (19, 30, 31). The main species observed is a 30-kDa species that corresponds to the functional domain of Ure2p (13, 19). Overall, the different species generated upon PK treatment of either soluble or aggregated *Sc* or *Sp*Ure2p are populated in the same quantity under the same conditions for the two proteins. It has been reported that extensive digestion of *Sc*Ure2p fibers with proteinase K leads to the production of a fuzzy band of low molecular weight corresponding to the prion domain (22). In our hands, we could not detect such a smear, even after adding additional proteinase K or incubating *Sc* or *Sp*Ure2p filaments for a longer period (13) (and data not shown). In an attempt to detect this prion domain, the proteinase K fragments were also examined by a Western blot analysis (Fig. 4*C*). The antibodies used to reveal the different fragments generated by the digestion of *Sp*Ure2p filaments with proteinase K permit the identification of the fragments previously identified by the staining procedure, but could not permit the identification of the prion domain.

Comparison of Time Course of Amyloid Fibril Formation for Sc and SpUre2—Fibril formation for *Sp* and *Sc*Ure2p was monitored by ThT fluorescence under various conditions of temperature, with and without agitation. Like *Sc*Ure2p, *Sp*Ure2p showed an increase in ThT fluorescence, indicating formation of amyloid-like structure, with a sigmoidal time course (Fig. 5). When GPx activity of *Sp*Ure2p was monitored during the course of fibril formation, the enzymatic activity of the sample was observed to disappear from the supernatant fraction and appear instead in the pellet fraction, concomitant with the formation of amyloid-like fibrils as monitored by ThT (supplemental Fig. S4). The total enzymatic activity of the sample remained almost constant. This result is essentially identical to that reported previously for *Sc*Ure2p (17). When the proteins were incubated in parallel without agitation, the time course for the two proteins was similar. Interestingly, when the proteins were incubated in parallel with agitation, the lag time for both proteins decreased, but the effect was greater for *Sp*Ure2p, and the relative ThT fluorescence became lower for *Sc*Ure2p. The difference in lag time became more marked as the shaking speed was increased, until at the highest shaking speeds (1000–1500 rpm), *Sc*Ure2p showed little increase in ThT fluorescence (Fig. 5). The same phenomenon was observed at 10 °C (Fig. 5) and at 37 °C (data not shown). When fibril samples produced under these conditions were examined by EM, the *Sc*Ure2p sample showed only short, poorly formed fibrils (Fig. 5). In contrast,

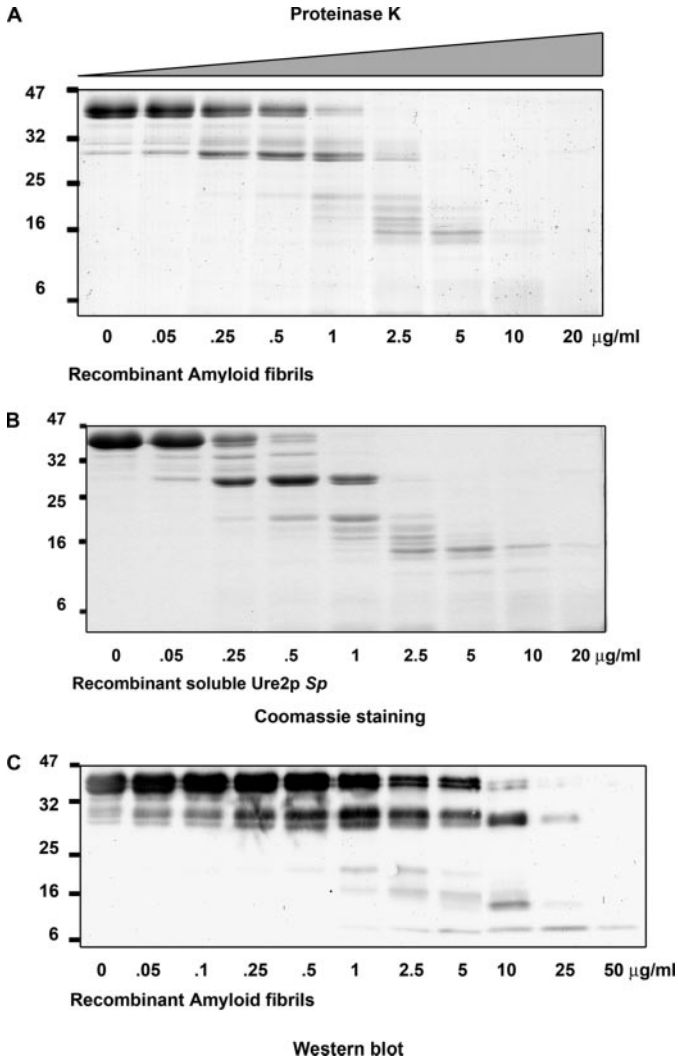

FIGURE 4. **Limited proteolysis of soluble and aggregated *Sp*Ure2p.** *A*, amyloid fibrils were digested with increasing concentrations of proteinase K for 15 min at 37 °C. Samples were analyzed by SDS-PAGE with Coomassie Blue staining. The *numbers* on the *vertical axis* denote the masses of marker proteins (kDa). *B*, controlled proteolysis of recombinant soluble Ure2p *Sp*. Recombinant soluble *Sp*Ure2p was digested in the presence of various proteinase K concentrations for 15 min at 37 °C. Samples were analyzed by SDS-PAGE followed by Coomassie Blue staining. The *numbers* on the *vertical axis* denote the masses of marker proteins (kDa). *C*, amyloid fibrils were analyzed by SDS-PAGE followed by a Western blot analysis with an antibody raised against full-length Ure2p.

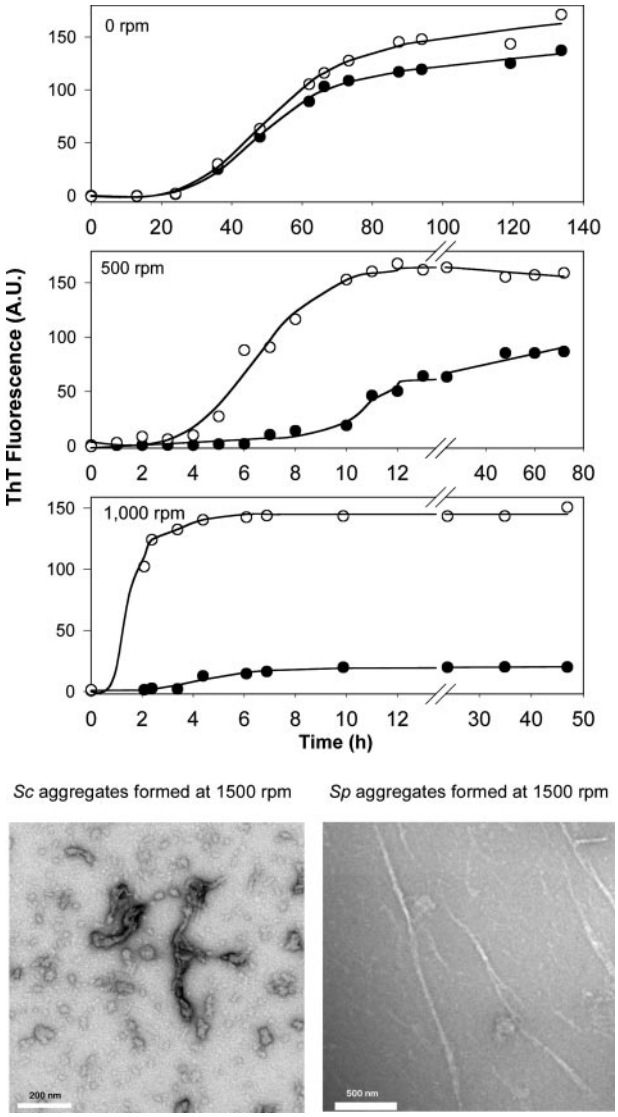

FIGURE 5. **Comparison of the time course of fibril formation for *S. cerevisiae* of *S. paradoxus* Ure2p, monitored by ThT binding.** 30 μM *S. paradoxus* (○) and *S. cerevisiae* (●) Ure2p in 50 mM Tris-HCl, pH 8.4, 200 mM NaCl, incubated at 10 °C. *Top graph*, without agitation. *Middle graph*, shaking at 500 rpm. *Bottom graph*, shaking at 1000 rpm. *Lower panel*, EM images of Sc and Sp fibrils formed under conditions of strong agitation (1500 rpm).

*Sp*Ure2p incubated in parallel under the same conditions showed abundant long fibrillar structures (Fig. 5). Agitation is thought to increase the rate of fibril growth by fragmenting the fibrils and thus generating additional fibril ends from which growth can take place. At very high shaking speeds, it appears that the *Sc*Ure2p fibrils are partially destroyed (or cannot be generated as readily), and so ThT fluorescence is reduced. In contrast, the *Sp* fibrils are significantly more resistant to mechanical force.

In Vivo Comparison of Sp and ScUre2p Aggregates—During the course of amyloid formation, aliquots of *Sp*Ure2p were analyzed for their capacity to induce [URE3] once introduced in wild-type CC30 yeast cells. Yeast spheroplasts, which are auxotrophic for leucine, were co-transformed with the sonicated aliquots together with a LEU2 plasmid. Leu+ transformants were tested for the presence of [URE3] by their capacity to grow in the presence of USA as sole precursor of UMP. The prion character was further assessed by the phenotypic reversibility of the growth on USA medium after having treated the cells with 5 mM GdnHCl. The results (supplemental Fig. S5) clearly demonstrate that *Sp*Ure2p amyloid is capable of infectivity, suggesting that its inability to propagate the prion state stems from an inability to generate new transmissible seeds rather than a fundamental difference in amyloid structure. Because *Sc* and *Sp* Ure2p amyloids made *in vitro* are both infectious, it is of interest to analyze whether any difference in aggregate structure is observed *in vivo*. Overexpression of *Sc*Ure2-GFP in [URE3] yeast cells permits the aggregation process to be followed. As previously shown (32), this process leads to the formation of a large globular aggregate (Fig. 6). When *Sp*Ure2-GFP is expressed instead of *Sc*Ure2-GFP, the kinetics of aggregation were more rapid. After 3 h, most of the cells show one large punctate focus (Fig. 6). A more dramatic difference was found after 24 h of *Sp*Ure2-GFP expression. In more than 80% of the yeast cells, a jellyfish-like structure was observed instead of the globular aggregate found when *Sc*Ure2-GFP is expressed. This branching structure is indeed compatible with a higher capacity for *Sp*Ure2p to form fibrillar structures and to resist fragmentation under these experimental conditions.

DISCUSSION

The conservation of prion properties through evolution is of interest to analyze the role of this mechanism in the living world. The two most intensively studied yeast prions [PSI] and [URE3] are not conserved in the same way. [PSI] can be propagated in *S. cerevisiae* by expressing Sup35 from distantly related hemiascomycete yeasts (9, 33–35), whereas [URE3] failed to be propagated by expressing Ure2p of *K. lactis*, a milk-loving yeast, believed to have diverged from the *Saccharomyces* clade at least 150 million years ago (10). A closer yeast species (*S. paradoxus*) possesses an intriguing *URE2* gene. When overexpressed in *S. cerevisiae*, the corresponding protein cannot induce [URE3] although its N-terminal domain expressed alone increased dramatically the rate of appearance of [URE3] in the same way as a *bona fide* "prion forming domain" (10). When *S. paradoxus* is used as the host for *S. cerevisiae* Ure2p expression, we were able to observe the [URE3] phenotype whereas this prion phenotype could not be observed at the same frequency when *S. paradoxus* Ure2p was expressed (12). The prion formation capacity is therefore clearly restricted to the primary sequence of the protein rather than to species-specific cellular factors involved in this mechanism.

The prion phenotypes [PSI] and [URE3] observed *in vivo* can be induced by transforming yeast cells with amyloid fibrils made *in vitro* from Sup35 or Ure2p, respectively (4, 5, 29, 36). The amyloidogenic properties of these proteins are enciphered into their N-terminal "prion forming domains" which are rich in asparagine and glutamine. Because *Sp*Ure2p cannot form a prion *in vivo* (although it contains an efficient PFD), it was therefore of interest to analyze its biochemical properties *in vitro*.

We first investigated the folding of *Sp*Ure2p purified under native conditions by a variety of methods. Because the prion domain of *Sp*Ure2p is inactive *in cis* (when linked to the remaining functional domain), one could expect that this inactivity might be caused by a stronger interaction between this N-terminal poorly structured domain and the rest of the protein.

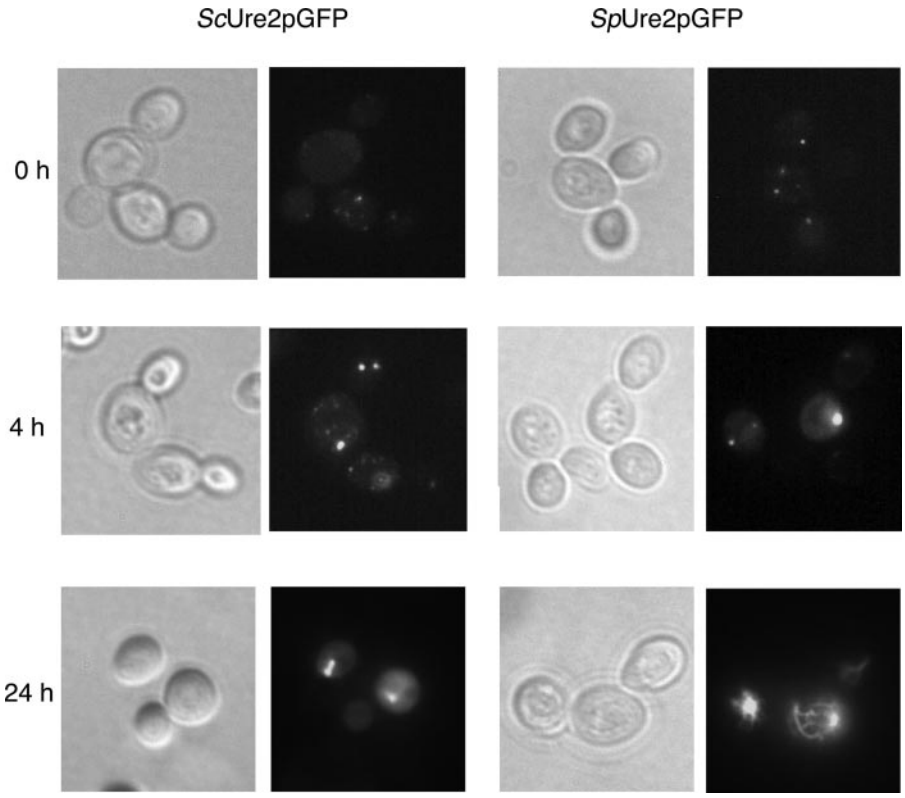

FIGURE 6. **Dynamics of the fluorescent aggregates in [URE3] cells during *Sc* or *Sp*Ure2-GFP overexpression.** [URE3] yeast cells were transformed with pYe2T-*sc*URE2GFP or pYe2T-*sp*URE2GFP plasmids. Cells were grown overnight on raffinose medium. 2% galactose was then added, to induce the Ure2-GFP expression, and cells were observed at different times after galactose addition.

Genetic (37) and biochemical (38, 39) experiments have suggested the existence of such an interaction in *Sc*Ure2p. However, direct experiments based on NMR and surface plasmon resonance (40) failed to confirm the existence of such an interaction. Our current work will not help to elucidate this conundrum because the behavior of the orthologous *Sp*Ure2 protein is indistinguishable from the genuine *Sc*Ure2p. The loss of prion function of *Sp*Ure2p *in vivo* is therefore probably not caused by a particular structure adopted by the PFD in the soluble form of the protein. This is in agreement with previous published results because these two proteins are identical in their functional domain (from Met^{95} to the end), while the remaining PFD (in which very few differences are found, supplemental Fig. S1) does not play any role in the overall structure and stability of the protein (14, 15). We next analyzed the stability of the protein. In the presence of increasing concentrations of guanidium hydrochloride, both *Sp* and *Sc*Ure2p exhibit the same denaturation propensity. All these experiments clearly show that the difference in prion forming behavior of *Sc* and *Sp*Ure2p is not caused by a difference in the folding of the soluble forms of the proteins. We therefore continued to apply further approaches to highlight subtle differences that must exist because these two proteins behave differently *in vivo*.

Next, we examined the amyloid propensity of *Sp*Ure2p. *A priori*, we expected a complete inability of *Sp*Ure2p to form any amyloid structure because this property is intimately linked to the prion formation mechanism. Unexpectedly, we found that the protein switches spontaneously from the soluble state to a largely aggregated structure. EM observation of these aggregates allowed the identification of the typical filamentous structures that are observed during *Sc*Ure2p aggregation. Moreover, *Sp*Ure2 fibril formation could be observed under many different conditions. This result indicates an efficient propensity for both *Sp* and *Sc*Ure2p to form filamentous amyloid-like structure.

An interesting feature of *Sc*Ure2p fibrils is that native-like globular structure and enzyme activity is maintained within the fibrils (17, 41, 42). To examine whether this is also the case for *Sp*Ure2 fibrils, we compared the susceptibility to limited protease digestion and the enzyme activity of the soluble and fibrillar forms of the protein. As found previously for *Sc*Ure2p under identical conditions the soluble and aggregated forms showed remarkably similar protease digestion patterns, and enzyme activity was maintained in the fibrillar state. At this level of observation, *Sp* and *Sc*Ure2p behave identically. The functional C-terminal domain appears to have a common structure in both soluble and fibrillar states. However, these proteins profoundly differ *in vivo* in their prion formation properties. This could be simply explained if *Sp*Ure2p amyloid fibrils were not capable of infectivity. However, we demonstrated that when the protein assembled *in vitro* into amyloid structure is introduced in wild type yeast cells, it has the capacity to switch endogenous *Sc*Ure2p into its prion shape. This experiment establishes unambiguously the infectious capacity of *Sp*Ure2p amyloid and suggests that the lack of prion behavior for *Sp*Ure2p results not from any fundamental difference in structure, but rather from an inability to reliably propagate the prion state. Recently, a model has been proposed to describe prion strains (43). This model highlights the importance of the kinetics of amyloid formation and in particular its rate of growth and fragmentation. The capacity to be infectious is therefore because of the rate of synthesis, but also to the fragility of the aggregates formed. Possible explanations for the particular behavior of *Sp*Ure2p could therefore be a difference either in the rate of amyloid growth or in the brittleness of the aggregates. The kinetics of *Sp* and *Sc*Ure2p fibril formation based on ThT fluorescence shows a classical sigmoidal curve. Interestingly, without agitation, both curves overlap, indicating a similar propensity for the proteins to switch from the soluble to the amyloid state. Upon mild agitation, the fragmentation of amyloid fibrils formed early generates new seeds and decreases the lag time. In contrast, when incubated under strong agitation, the specific signal because of the interaction between *Sc*Ure2p amyloid fibrils, and ThT was significantly reduced.

Direct observation by EM links this failure to the reduced ability to maintain fibrillar structure under conditions of strong agitation. *Sp*Ure2p shows quite different behavior under these conditions and a clear increase in ThT fluorescence over the time course is observed, which corresponds with the ability of the protein to form long fibrils, as observed by EM. The *Sp* fibrils seem to be significantly more resistant to mechanical force. This then suggests a mechanism for the inability of the *Sp*Ure2p to act as a propagatable species in yeast: if the prion aggregates are too robust to be fragmented, then there will be insufficient seeds to allow efficient propagation at cell division, and so the prion state would always be lost before it could be detected. This explanation is supported by the capacity of *Sp*Ure2-GFP to assemble into a distinctive structure in the presence of the prion isoform of *Sc*Ure2p. These "jellyfish" structures are not observed with *Sc*Ure2-GFP and have never been reported for other yeast prions. Without further characterization of these structures, it is difficult to speculate about their biochemical organization. However, it is tempting to postulate that they may stem from the propensity of *Sp*Ure2p to polymerize under conditions that would lead *Sc*Ure2p to form large amorphous aggregates. *In vivo*, the formation of [URE3] requires the presence of active chaperones and is completely dependent on the presence of Hsp104. Recently, an *in vitro* system has permitted clarification of the role of this protein on prion formation and infectivity (36). If the higher propensity of *Sp*Ure2p to form amyloid makes it a "cul-de-sac" for prion formation, we wondered whether overexpression of HSP104 might rescue the prion mechanism. However, when HSP104 is overexpressed in CC30 strains, together with *Sp*Ure2p (under the conditions previously used, Ref. 10), the yeast cells did not gain the capacity to form [URE3] (data not shown). Of course, *Sc*Ure2p in the [URE3] form is also insensitive to overexpression of HSP104 (44), therefore this lack of effect is perhaps unsurprising. We now have to identify the amino acids that are specifically involved in this non-infectious effect. Elucidating the mechanism by which these amino acids contribute to this effect remains also an exciting challenge and may shed light on the mechanism of Ure2p prion formation.

Acknowledgments—We thank Prof. I. Lascu for his valuable help with CD experiments, Dr. M. Castroviejo for his help during SEC experiments, F. Lefebvre for the construction of the GFP fusion, and Dr. B. Salin and the IBP EM Centre for assistance with EM.

REFERENCES

1. Sparrer, H. E., Santoso, A., Szoka, C. F., Jr., and Weissman, J. S. (2000) *Science* **289,** 595–599
2. Griffith, J. S. (1967) *Nature* **215,** 1043–1044
3. Prusiner, S. B. (1982) *Science* **216,** 136–144
4. Tanaka, M., Chien, P., Naber, N., Cooke, R., and Weissman, J. S. (2004) *Nature* **428,** 323–328
5. King, C. Y., and Diaz-Avalos, R. (2004) *Nature* **428,** 319–323
6. Masison, D., and Wickner, R. B. (1995) *Science* **270,** 93–95
7. Beck, T., and Hall, M. N. (1999) *Nature* **402,** 689–692
8. True, H. L., and Lindquist, S. L. (2000) *Nature* **407,** 477–483
9. Nakayashiki, T., Ebihara, K., Bannai, H., and Nakamura, Y. (2001) *Mol. Cell* **7,** 1121–1130
10. Baudin-Baillieu, A., Fernandez-Bellot, E., Reine, F., Coissac, E., and Cullin, C. (2003) *Mol. Biol. Cell* **14,** 3449–3458
11. Edskes, H. K., and Wickner, R. B. (2002) *Proc. Natl. Acad. Sci. U. S. A.* **99,** Suppl. 4, 16384–16391
12. Talarek, N., Maillet, L., Cullin, C., and Aigle, M. (2005) *Genetics* **171,** 23–34
13. Ripaud, L., Maillet, L., Immel-Torterotot, F., Durand, F., and Cullin, C. (2004) *J. Biol. Chem.* **279,** 50962–50968
14. Thual, C., Bousset, L., Komar, A. A., Walter, S., Buchner, J., Cullin, C., and Melki, R. (2001) *Biochemistry* **40,** 1764–1773
15. Perrett, S., Freeman, S. J., Butler, P. J., and Fersht, A. R. (1999) *J. Mol. Biol.* **290,** 331–345
16. Zhu, L., Zhang, X. J., Wang, L. Y., Zhou, J. M., and Perrett, S. (2003) *J. Mol. Biol.* **328,** 235–254
17. Bai, M., Zhou, J. M., and Perrett, S. (2004) *J. Biol. Chem.* **279,** 50025–50030
18. Flohé, L., and Günzler, W. A. (1984) *Methods Enzymol.* **105,** 114–121
19. Thual, C., Komar, A. A., Bousset, L., Fernandez-Bellot, E., Cullin, C., and Melki, R. (1999) *J. Biol. Chem.* **274,** 13666–13674
20. Taylor, K. L., Cheng, N., Williams, R. W., Steven, A. C., and Wickner, R. B. (1999) *Science* **283,** 1339–1343
21. Schlumpberger, M., Wille, H., Baldwin, M. A., Butler, D. A., Herskowitz, I., and Prusiner, S. B. (2000) *Protein Sci.* **9,** 440–451
22. Baxa, U., Taylor, K. L., Wall, J. S., Simon, M. N., Cheng, N., Wickner, R. B., and Steven, A. C. (2003) *J. Biol. Chem.* **278,** 43717–43727
23. Baxa, U., Cheng, N., Winkler, D. C., Chiu, T. K., Davies, D. R., Sharma, D., Inouye, H., Kirschner, D. A., Wickner, R. B., and Steven, A. C. (2005) *J. Struct. Biol.* **150,** 170–179
24. Giartosio, A., Erent, M., Cervoni, L., Moréra, S., Janin, J., Konrad, M., and Lascu, I. (1996) *J. Biol. Chem.* **271,** 17845–17851
25. Carpenter, J. F., and Crowe, J. H. (1988) *Cryobiology* **25,** 244–255
26. Vuillard, L., Braun-Breton, C., and Rabilloud, T. (1995) *Biochem. J.* **305,** 337–343
27. Baskakov, I., and Bolen, D. W. (1998) *J. Biol. Chem.* **273,** 4831–4834
28. Bousset, L., Belrhali, H., Melki, R., and Morera, S. (2001) *Biochemistry* **40,** 13564–13573
29. Brachmann, A., Baxa, U., and Wickner, R. B. (2005) *EMBO J.* **24,** 3082–3092
30. Komar, A. A., Lesnik, T., Cullin, C., Guillemet, E., Ehrlich, R., and Reiss, C. (1997) *FEBS Lett.* **415,** 6–10
31. Bousset, L., Redeker, V., Decottignies, P., Dubois, S., Le Marechal, P., and Melki, R. (2004) *Biochemistry* **43,** 5022–5032
32. Ripaud, L., Maillet, L., and Cullin, C. (2003) *EMBO J.* **22,** 5251–5259
33. Chernoff, Y. O., Galkin, A. P., Lewitin, E., Chernova, T. A., Newnam, G. P., and Belenkiy, S. M. (2000) *Mol. Microbiol.* **35,** 865–876
34. Kushnirov, V. V., Kochneva-Pervukhova, N. V., Chechenova, M. B., Frolova, N. S., and Ter-Avanesyan, M. D. (2000) *EMBO J.* **19,** 324–331
35. Resende, C., Parham, S. N., Tinsley, C., Ferreira, P., Duarte, J. A., and Tuite, M. F. (2002) *Microbiology* **148,** 1049–1060
36. Shorter, J., and Lindquist, S. (2006) *Mol. Cell* **23,** 425–438
37. Fernandez-Bellot, E., Guillemet, E., and Cullin, C. (2000) *EMBO J.* **19,** 3215–3222
38. Fay, N., Redeker, V., Savistchenko, J., Dubois, S., Bousset, L., and Melki, R. (2005) *J. Biol. Chem.* **280,** 37149–37158
39. Fernandez-Bellot, E., Guillemet, E., Baudin-Baillieu, A., Gaumer, S., Komar, A. A., and Cullin, C. (1999) *Biochem. J.* **338,** 403–407
40. Pierce, M. M., Baxa, U., Steven, A. C., Bax, A., and Wickner, R. B. (2005) *Biochemistry* **44,** 321–328
41. Baxa, U., Speransky, V., Steven, A. C., and Wickner, R. B. (2002) *Proc. Natl. Acad. Sci. U. S. A.* **99,** 5253–5260
42. Bousset, L., Thomson, N. H., Radford, S. E., and Melki, R. (2002) *EMBO J.* **21,** 2903–2911
43. Tanaka, M., Collins, S. R., Toyama, B. H., and Weissman, J. S. (2006) *Nature* **442,** 585–589
44. Moriyama, H., Edskes, H. K., and Wickner, R. B. (2000) *Mol. Cell Biol.* **20,** 8916–8922